Localization and the Kosterlitz-Thouless Transition in Disordered Graphene

Yan-Yang Zhang,[1] Jiangping Hu,[1] B. A. Bernevig,[2] X. R. Wang,[3] X. C. Xie,[4,5] and W. M. Liu[4]

[1]*Department of Physics, Purdue University, West Lafayette, Indiana 47907, USA*
[2]*Princeton Center for Theoretical Science, Jadwin Hall, Princeton University, Princeton, New Jersey 08544, USA*
[3]*Physics Department, The Hong Kong University of Science and Technology, Clear Water Bay, Hong Kong SAR, China*
[4]*Institute of Physics, Chinese Academy of Sciences, Beijing 100080, China*
[5]*Department of Physics, Oklahoma State University, Stillwater, Oklahoma 74078, USA*

(Received 14 October 2008; published 10 March 2009)

We investigate disordered graphene with strong long-range impurities. Contrary to the common belief that delocalization should persist in such a system against any disorder, as the system is expected to be equivalent to a disordered two-dimensional Dirac fermionic system, we find that states near the Dirac points are localized for sufficiently strong disorder (therefore inevitable intervalley scattering) and the transition between the localized and delocalized states is of Kosterlitz-Thouless type. Our results show that the transition originates from bounding and unbounding of local current vortices.

DOI: 10.1103/PhysRevLett.102.106401 PACS numbers: 71.30.+h, 72.10.−d, 72.15.Rn, 73.20.Fz

It is well known that the electronic spectrum of graphene can be approximately described by Dirac fermions [1–5], due to the linear dispersion relation near two inequivalent points $\mathbf{K}$ and $\mathbf{K}'$ at the corner of the Brillouin zone [4]. The relativistic dispersion gives rise to several remarkable phenomena. Unlike nonrelativistic Schrödinger fermions in two dimensions [6], Dirac fermions cannot be trapped by a barrier due to the Klein paradox [7]. Theories based on the two-dimensional (2D) single valley Dirac Hamiltonian also predict that Dirac fermions cannot be localized by disorder [2,8–10].

Most of the experimental and theoretical studies of graphene [3,11] have focused on the effect of the relativistic electronic dispersion on different phenomena such as Landau level structure or quantum Hall ferromagnetism. However, the validity of single valley Dirac fermion picture for disordered graphene is only approximate and relies on two premisses: (i) The spatial range of the impurities is long enough to avoid intervalley scattering effectively [2] (strong intervalley scattering can lead to localization [2,12,13]); (ii) Even within a single valley, the (linear dispersed) Dirac Hamiltonian is only valid near Dirac points $\mathbf{K}$ and $\mathbf{K}'$. The approximation cannot be carried out in a region with a strong impurity where the deviation from the Dirac point is large enough so that higher order corrections to the energy spectrum become relevant [2]. Therefore, the application of single valley Dirac Hamiltonian to disordered graphene is limited to weak long-range impurities. Indeed, localized states in disordered graphene near Dirac points have been observed experimentally [14] and numerically [15,16]. All the above beg the physical question: how does graphene behave in the presence of strong long-range impurities?

In this Letter, we calculate the scaling properties of disordered graphene with long-range impurities in the framework of a tight-binding model and finite-size scaling. Instead of delocalization we find that, in the presence of strong long-range impurities, states near the Dirac points are localized. Localization arises from enhanced intervalley scattering due to the deviation from Dirac dispersion in the strong impurity regime. We show numerical evidence for a marginal metal (scaling function $\beta = 0$) to insulator transition (MIT) as a function of the disorder strength and chemical potential. On the delocalized (marginal metallic) side, we find that the conductance is independent of the system size, which is a characteristic of the Kosterlitz-Thouless (K-T) [17] type transition in conventional 2D systems with random magnetic field [18,19]. We explicitly probe the Kosterlitz-Thouless transition nature of the MIT by identifying the bounding and unbounding vortex-antivortex local currents in the system.

The π electrons in graphene are described by the tight-binding Hamiltonian (TBH)

$$H = \sum_i V_i c_i^\dagger c_i + t \sum_{\langle i,j \rangle} (c_i^\dagger c_j + \text{H.c.}), \tag{1}$$

where $c_i^\dagger$ (c_i) creates (annihilates) an electron on site i with coordinate $\mathbf{r}_i$, t ($\sim$2.7 eV) is the hopping integral between the nearest neighbor carbon atoms with distance $a/\sqrt{3}$ ($a \sim 2.46$ Å is the lattice constant), and V_i is the potential energy. In the presence of disorder, V_i is the sum of contributions from N_I impurities randomly centered at $\{\mathbf{r}_m\}$ among N sites $V_i = \sum_{m=1}^{N_I} U_m \exp(-|\mathbf{r}_i - \mathbf{r}_m|^2/(2\xi))$, where U_m is randomly distributed within $(-W/2, W/2)$ in units of t. Different random configurations of graphene samples with same size, ξ, W and $n_i \equiv N_I/N$ constitute an ensemble with definite disorder strength. This model of disordered graphene has been widely used [20–22].

At zero temperature, the two terminal dimensionless conductance g_L of the sample at Fermi energy E_F is given by Landauer-Büttiker formula [23]: $g_L(E_F) = 2\text{Tr}(tt^\dagger)$, where t is the transmission matrix and the factor 2 accounts for spin degeneracy. This equation can be numerically

evaluated by recursive Green's function method [24] for systems with rather large size. For the purpose of scaling, the contact effect should be subtracted from g_L to yield the "intrinsic conductance", g, defined as $1/g = 1/g_L - 1/(2N_C)$, where N_C is the number of propagating channels at Fermi energy E_F and $1/(2N_C)$ is the contact resistance [25]. The conductance g then receives contributions solely from the bulk and thus has the same scaling property as if it were obtained by the transfer matrix method [26]. The scaling function [6,26]

$$\beta = \frac{d\langle \ln g \rangle}{d \ln L}, \tag{2}$$

$\langle \ldots \rangle$ being the average over random ensemble, is used to determine the localization properties; $\beta < 0$ and $\beta > 0$ correspond to the insulator and the metal, respectively.

We plot the size dependence of $\langle \ln g \rangle$ with $\xi = 1.73a$, $n_I = 1\%$, for different E_F and W in Fig. 1. The samples are set to be square shaped with length L. Periodic boundary conditions in the transverse direction are adopted to exclude the edge states of the zigzag edges [21]. The potential range ξ chosen here was supposed to be "long range" enough [2,21], and the scaling $\xi/L_x \sim 0$ is irrelevant. When $E_F < E_c = 0.1t$ [Fig. 1(a)] or $W > W_c = 2t$ [Fig. 1(b)], $\langle g \rangle$ is monotonically decreasing with increasing L, which means the wave functions are localized. Otherwise, when $E_F > E_c = 0.1t$ [Fig. 1(a)] or $W < W_c = 2t$ [Fig. 1(b)], $\langle \ln g \rangle$ curves for different sizes merge, suggesting a delocalized state with finite conductance in the thermodynamic limit. However, they are not real metals with $\beta > 0$. All the states with $W \in (0, W_c)$ are within the MIT region with $\beta = 0$. Even in the cases of extremely weak disorder with $W = 0.25t$ and $W = 0.1t$ [see the inset of Fig. 1(b)], except for a vanishing even-odd fluctuation, $\langle \ln g \rangle(L)$ does not seem to show a tendency to be increasing nor decreasing. In Fig. 2, the universal $\beta(\ln g)$ is plotted from the same data in Fig. 1, showing a critical conductance $\ln g_c \sim 0.4$ separating the delocalized states with $\beta = 0$ and localized states with $\beta < 0$. Approaching $\ln g_c$ from insulating side, the localization length diverges as $\lambda = \lambda_0 |W - W_c|^{-\nu}$, where $\nu = 4$ is equal to the inverse of the slope of $\beta(\ln g)$ at $(\ln g_c - 0)$ [26,27]. This phenomenon corresponds to a disorder-driven K-T type transition that has been observed in many disordered 2D systems [18,19,28]. As can be seen from Fig. 1(a) and the phase diagram (inset of Fig. 2), states in the low energy region are more easily localized.

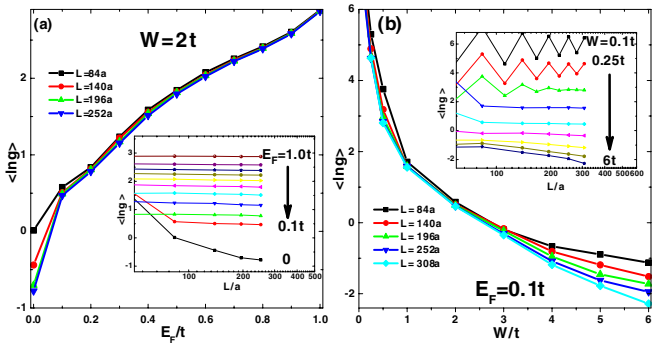

FIG. 1 (color online). The scaling of conductance for long-range disorder ($\xi = 1.73a$, $n_I = 1\%$): (a) $\langle \ln g \rangle$ as functions of the Fermi energy E_F with fixed disorder strength $W = 2t$ (note: the bandwidth is $6t$); (b) $\langle \ln g \rangle$ as functions of disorder strength W with fixed Fermi energy $E_F = 0.1t$. The insets are the same data plotted as functions of size L. Each $\langle \ln g \rangle$ is an average over $100 \sim 400$ random realizations.

The localization near the Dirac point is in contrast to the belief that Dirac fermions are robust against localization, especially in the presence of long-range impurities. In order to gain insight in the nature of the localization transition, we first turn back to the dispersion structure of realistic graphene.

$$E_{\pm}(\mathbf{q}) = \pm \frac{3ta}{2}|\mathbf{q}| \pm \frac{\sqrt{3}ta^2}{8}\sin(3\alpha(\mathbf{q}))|\mathbf{q}|^2 + O(q^3), \tag{3}$$

where $\mathbf{q} \equiv \mathbf{k} - \mathbf{K}$ and $\alpha(\mathbf{q}) \in [0, 2\pi)$ is the angle of vector $\mathbf{q}$. The first term in the right-hand side of (3) corresponds to the Dirac Hamiltonian, but nonlinear terms will be prominent when $\mathbf{q}$ (or E) is increased. For example, the angular dependence factor $\sin(3\alpha(\mathbf{q}))$ ("trigonal warping") breaks pseudotime reversal symmetry [5,10,21] restricted to each valley. When $|E| > t$, the linear approximation and double-valley structure collapses completely [see Figs. 3(g) and 3(h)]. Thus strong local potential of impurities might create non-Dirac scattering, which will lead to a tendency towards localization.

Now consider the simplest case of a single long-range impurity in the center of a graphene sheet. If intervalley coupling is effectively prohibited and the regime of Klein tunneling holds, there should be no bound states, no matter how high the potential barrier is [7]. After diagonalizing the Hamiltonian for a graphene sheet with N sites, the spatial extension of eigenstate $|\psi_n\rangle = \sum_{i=1}^{N} a_{ni} c_i^{\dagger}|0\rangle$ with eigenenergy E_n can be characterized by the participation ratio

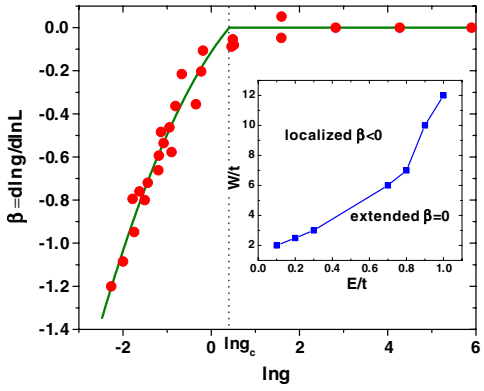

FIG. 2 (color online). The scaling function $\beta = \frac{d\langle \ln g \rangle}{d \ln L}$ obtained from the data in Fig. 1. The inset is the schematic phase diagram for $\xi = 1.73a$, $n_I = 1\%$.

$$R_n = \left(\sum_{i=1}^{N} a_{ni}^2\right)^2 \Big/ \left(N \sum_{i=1}^{N} a_{ni}^4\right). \quad (4)$$

For an extended state, R has a finite value (typically close to $1/3$ in the presence of disorder), whereas for a localized state R approaches zero proportional to $(1/N)$ [29]. The results for $\xi = 1.73a$ with different potential height $V \geq 0$ is plotted in Fig. 3. For small V [Fig. 3(a) and 3(b)], where the electronic behaviors inside and outside the barrier are Dirac-like [Fig. 3(e) and 3(f)], there are no bound states. When V is increased, bound states with small R begin to appear in the negative energy region near the Dirac point, as seen in Fig. 3(c). For positive injected energy [orange arrow with solid line in Fig. 3(g)], the electron is not far from **K** both inside and outside the barrier, so the regime of Klein tunneling is still valid and the electron cannot be trapped. On the other hand, for negative energy [orange arrow with dashed line in Fig. 3(g)], the electron sees a non-Dirac barrier (pointed by the yellow arrow). This causes strong non-Dirac scattering and localization around the impurity. When V is increased further [Fig. 3(h)], even electrons in the positive Dirac region will encounter strong non-Dirac scattering in the barrier and will be localized [Fig. 3(d)]. Note here when $E_F < 0$ [the orange arrow in Fig. 3(h)], the two valleys in the barrier merge, causing a possibility of remarkable intervalley scattering (see below). For negative V (not shown here), all the results are similar, except that the localized states now first appear in the positive region near Dirac point. The states near the Dirac point with low density of states will be more sensitive to disorder and will be localized first, as in the case of conventional disordered systems [24–26].

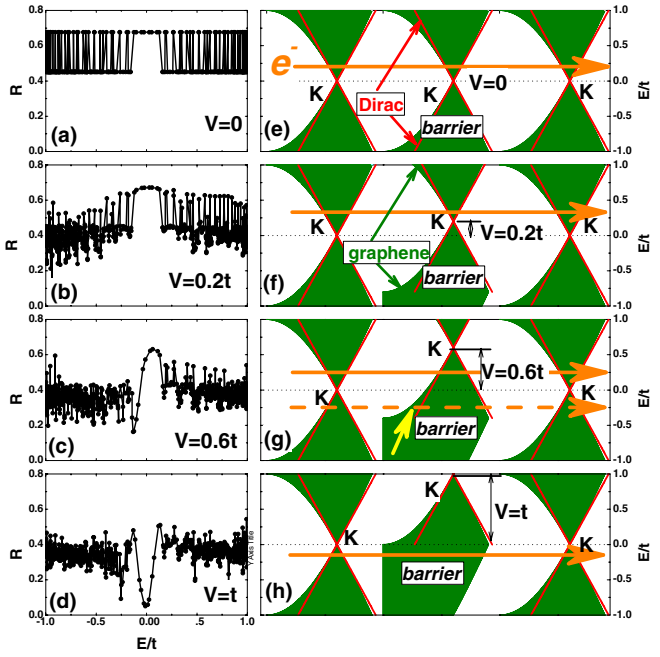

FIG. 3 (color online). Left column [(a)–(d)]: The participation ratio R as functions of energy E for a graphene with $N = 70 \times 40$, in the presence of a single impurity at the center with $\xi = 1.73a$ with different potential height $V \geq 0$. Right column [(e)–(h)]: Schematic diagrams of scattering process corresponding to their left counterparts. The electron is injected from the left, scattered by the barrier at the center and eventually transmitted to the right (thick orange arrows). The red lines mark the Dirac dispersion $E_{\pm}(\mathbf{k}) = \pm \frac{3ta}{2}|\mathbf{k} - \mathbf{K}|$ and the olive part is that for graphene calculated from TBH. Note the discrepancies between them at high energy.

This localization induced by long range but strong impurities is directly correlated with intervalley scattering. The valley-resolved scattering amplitude A can be calculated by a generalization of Ando's method [30]. The sum of all the scattering amplitudes is equal to the propagating channels at Fermi energy E_F: $N_C = A_{\text{intra}} + A_{\text{inter}}$. The results are shown in Fig. 4. It is clear now that the localization observed in Fig. 1 ($W > 2$) and Fig. 3 ($V > 1$) is induced by remarkable impurity-assisted intervalley scattering, which is consistent with theoretical prediction that, this type of scattering will lead graphene into the common regime of Anderson localization [12]. For a strong enough impurity barrier ($V > t$), this intervalley scattering is a result of non-Dirac behavior of the honeycomb lattice in the high energy region and cannot be avoided by simply increasing the potential range ξ.

One question remains: Why is the MIT in disordered graphene of K-T type? The K-T transition is a typical topological transition which has been understood as unbounding of vortex-anti-vortex pairs [17]. For instance, in the high temperature phase 2D XY model, a plasma of unbounded vortices and antivortices of local spins gives rise to an exponential decay of spin correlation function; in the low temperature phase, vortices and antivortices are bound to each other, leading to a power law correlation function. This can be clearly seen in the present problem if the local currents are identified with local spins in XY model.

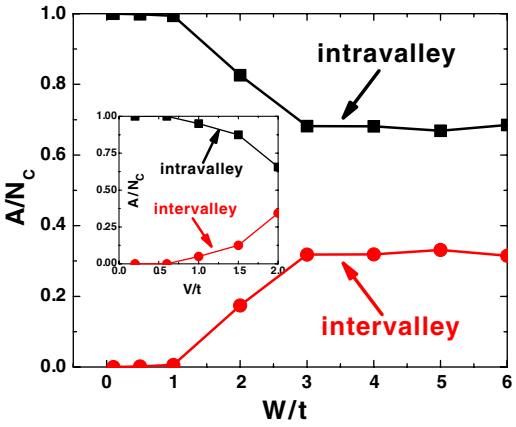

FIG. 4 (color online). The normalized scattering amplitudes A_{intra}/N_C and A_{inter}/N_C as functions of W. Each point is an average over 100 samples on a square graphene sheet with 112×64 sites. Other parameters are same with Fig. 1(b). The inset is the results corresponding to the single-impurity case in Fig. 3 at $E_F = 0$.

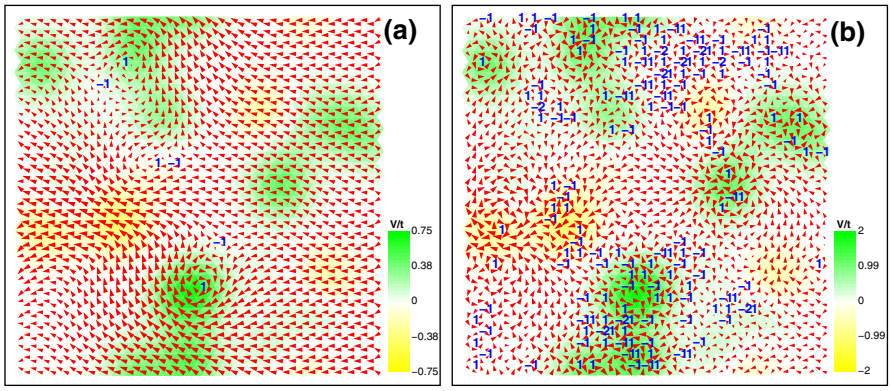

FIG. 5 (color online). Typical configurations of local currents $\mathbf{i}_n$ (red arrows) and potential V_n (color contour) on two sides of K-T type MIT with $N = 56 \times 32$ sites, $\xi = 1.73a$, $n_I = 1\%$ and $E_F = 0.1t$. (a) $W = 1.1t$ (delocalized); (b) $W = 2.9t$ (localized). The size of arrows is proportional to the logarithm of current value. Carbon hexagons with topological charge $n \neq 0$ are marked explicitly with blue numbers.

The bond current vector $\mathbf{i}_{l\to m}(E_F)$ per unit energy pointing along the bond between sites l and m can be calculated using Green's functions [23,31,32]. It is more convenient to investigate the "current flow vector" $\mathbf{i}_l = \sum_m \mathbf{i}_{l\to m}$ defined on site l, where the vectorial summation is taken over the nearest neighbors of site l [31]. The current flow $\mathbf{i}_l$ is a vector with angle $\theta_l \in [0, 2\pi)$. The topological charge n of local currents on a closed path can now be defined as usual: $n = \frac{1}{2\pi} \oint \nabla\theta \cdot d\boldsymbol{l}$. In Fig. 5, typical distributions of local currents on both sides of MIT are plotted. As expected from the K-T picture, in the delocalized phase [Fig. 5(a)], vortices ($n > 0$) and antivortices ($n < 0$) are closely bounded, corresponding to the "low temperature" phase of 2D XY model with quasi-long-range correlations. In the localized phase [Fig. 5(b)], there are a large number of current vortices and antivortices. Many of them are unbounded, corresponding to the "high temperature" phase of 2D XY model without long-range correlations. This offers an explicit picture of the microscopic origin of the disorder-driven K-T transition in graphene.

In conclusion, we find a Kosterlitz-Thouless type marginal metal-to-insulator transition as a function of disorder strength or Fermi energy in disordered graphene with strong long-range impurities. We explicitly demonstrate the KT nature of transition by showing the bounding and unbounding of local current vortexes. Recently, the MIT near the neutral point of graphene has been observed in graphene nanoribbons [14] which are quasi-one-dimensional systems. Our results can be tested in experiments with large nanoribbon radius.

We thank D.-X. Yao, W.-F. Tsai, C. Fang, and Professor C. W. J. Beenakker for useful discussions. X. C. X. was supported by 973 Program Project No. 2009CB929101. Y. Y. Z. and J. P. H. were supported by the NSF under Grant No. PHY-0603759. W. M. L. was supported by NSFC under Grant No. 60525417, the NKBRSFC under Grant No. 2006CB921400. X. R. W. was supported by HKUST UGC/RGC Grants No. RPC07/08.SC03.

[1] P. R. Wallace, Phys. Rev. **71**, 622 (1947).
[2] T. Ando and T. Nakanishi, J. Phys. Soc. Jpn. **67**, 1704 (1998); T. Ando *et al.*, *ibid.* **67**, 2857 (1998).
[3] K. S. Novoselov *et al.*, Nature (London) **438**, 197 (2005).
[4] C. K. Kane, Nature (London) **438**, 168 (2005).
[5] A. F. Morpurgo and F. Guinea, Phys. Rev. Lett. **97**, 196804 (2006).
[6] E. Abrahams *et al.*, Phys. Rev. Lett. **42**, 673 (1979).
[7] M. I. Katsnelson *et al.*, Nature Phys. **2**, 620 (2006).
[8] K. Ziegler, Phys. Rev. Lett. **80**, 3113 (1998).
[9] J. H. Bardarson *et al.*, Phys. Rev. Lett. **99**, 106801 (2007).
[10] K. Nomura *et al.*, Phys. Rev. Lett. **99**, 146806 (2007).
[11] B. Huard *et al.*, Phys. Rev. Lett. **98**, 236803 (2007).
[12] A. Altland, Phys. Rev. Lett. **97**, 236802 (2006).
[13] S.-J. Xiong and Y. Xiong, Phys. Rev. B **76**, 214204 (2007).
[14] S. Adam *et al.*, Phys. Rev. Lett. **101**, 046404 (2008).
[15] V. M. Pereira *et al.*, Phys. Rev. Lett. **96**, 036801 (2006).
[16] M. Amini *et al.*, arXiv:0806.1329.
[17] J. M. Kosterlitz and D. J. Thouless, J. Phys. C **6**, 1181 (1973).
[18] X. C. Xie *et al.*, Phys. Rev. Lett. **80**, 3563 (1998).
[19] W.-S. Liu *et al.*, Phys. Rev. B **60**, 5295 (1999).
[20] A. Rycerz *et al.*, Europhys. Lett. **79**, 57003 (2007).
[21] K. Wakabayashi *et al.*, Phys. Rev. Lett. **99**, 036601 (2007).
[22] C. H. Lewenkopf *et al.*, Phys. Rev. B **77**, 081410(R) (2008).
[23] S. Datta, *Electronic Transport in Mesoscopic Systems* (Canmbridge University Press, Cambridge, England, 1995).
[24] A. MacKinnon, Z. Phys. B **59**, 385 (1985).
[25] D. Braun *et al.*, Phys. Rev. B **55**, 7557 (1997).
[26] K. Slevin *et al.*, Phys. Rev. Lett. **86**, 3594 (2001).
[27] B. Shapiro, Philos. Mag. B **56**, 1031 (1987).
[28] V. Kalmeyer *et al.*, Phys. Rev. B **48**, 11 095 (1993); S.-C. Zhang and D. P. Arovas, Phys. Rev. Lett. **72**, 1886 (1994).
[29] J. T. Edwards and D. J. Thouless, J. Phys. C **5**, 807 (1972).
[30] T. Ando, Phys. Rev. B **44**, 8017 (1991).
[31] L. P. Zârbo and B. K. Nikolić, Europhys. Lett. **80**, 47 001 (2007).
[32] Y. Y. Zhang *et al.*, Phys. Rev. B **78**, 155413 (2008).